ACS APPLIED MATERIALS & INTERFACES

Research Article

www.acsami.org

Robust Microzip Fastener: Repeatable Interlocking Using Polymeric Rectangular Parallelepiped Arrays

Chanseok Lee,[†,‡,⊥] Sang Moon Kim,[†,‡,⊥] Young Joo Kim,[†] Yong Whan Choi,[†,‡] Kahp-Yang Suh,[†,‡,∥] Changhyun Pang,*[,§] and Mansoo Choi*[,†,‡]

[†]Department of Mechanical and Aerospace Engineering, Seoul National University, Seoul 151-742, Republic of Korea

[‡]Global Frontier Center for Multiscale Energy Systems, Seoul National University, Seoul 151-744, Republic of Korea

[§]School of Chemical Engineering, Sungkyunkwan University (SKKU), Suwon 440-746, Republic of Korea

Supporting Information

ABSTRACT: We report a highly repeatable and robust microzip fastener based on the van der Waals force-assisted interlocking between rectangular parallelepiped arrays. To investigate zipperlike interlocking behaviors, various line arrays were fabricated with three different spacing ratios (1, 3, and 5 of 800 nm in width) and width of parallelepipeds (400 nm, 800 nm, and 5 μm with the spacing ratio of 1). In addition, the different rigidity of line arrays was inspected for a repeatable microzip fastener. The normal and shear locking forces were measured with variation of the material rigidity as well as geometry of the array, in good agreement with a proposed theory based on the contact area and force balance. The maximum adhesion forces as high as ~8.5 N cm^{-2} in the normal direction and ~29.6 N cm^{-2} in the shear direction were obtained with high stability up to 1000 cycles. High stability of our fastening system was confirmed for preventing critical failures such as buckling and fracture in practical applications.

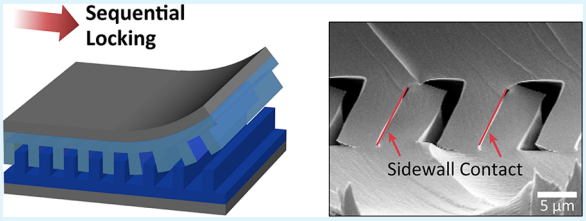

KEYWORDS: *zipperlike, dry adhesive, interlocking, line pattern, robust*

1. INTRODUCTION

Repeatable fastening and fixation ability is known as one of the essential features for many living organisms in nature, which can be achieved by various attachment systems exploiting mechanical, electrochemical, and capillary-based mechanisms.[1,2] For the repeatable attachment, a wide range of structure-based locking apparatus have been employed for various species, such as the hook structure of the plants[3,4] and wing locking system in beetles.[5,6] Recently, a gearlike structure was found in plant hoppers, which enables synchronized movements of each leg for the jumping process.[7] Such biological fastening systems have been investigated to elucidate the principle of microscopic mechanical locking effects. In most cases, van der Waals forces between rough surfaces play a key role in exerting stable and repeatable adhesion. Various artificial fastening and tunable adhesion systems have been introduced with various shapes and materials such as core−shell nanowire forest,[8,9] carbon nanotubes (CNTs),[10−12] polymer micro/nanofibers,[13−15] elastomeric pyramidal structures,[16,17] sharp particles,[18] and rippled structures.[19−21]

In general, densely populated micro- or nanostructures with high aspect ratio (AR) have been used so that the van der Waals-assisted adhesion can be maximized by larger contact area and surface compliance.[13,22−25] However, it is known that the intrinsic mechanical instability of the high aspect ratio structures is a major obstacle for a high robustness of repeatable fastener.[24,26] For example, nanohairs or nanowires are known to be prone to mechanical failures including permanent bending, irreversible buckling, and lateral collapsing when external load is applied.[11,12,14] To reduce the structural weakness of the adhesive system, several techniques have been proposed such as employing complicated hierarchical assemblies,[12,27] additional surface treatments,[9,28,29] and sharp zinc oxide particles.[18] Although the reported techniques enhanced the adhesion strength, further development of a simple and robust structure with high repeatability is still required for the realization of practical and stable fastening systems.

Here, we report a highly stable, van der Waals force-assisted, and zipperlike interlocking adhesive with high shear and normal adhesion forces based on the simple line arrays of low aspect ratio (AR ~2) which is defined as height of parallelepiped divided by width of parallelepiped. Unlike the nanofiber-based or nanowire-based interlocker, the critical fracture and buckling of line structures was not observed due to the geometric stability of the low aspect ratio structures. Such line arrays are cost-effective and can be easily replicated using ultraviolet (UV) curable materials. In order to investigate the mechanical behavior of the parallelepiped interlocking devices, several different geometries were applied by changing the spacing ratio (SR 1, 3, and 5, defined as gap between two neighboring parallelepipeds divided by width of the parallelepiped) of line

Received: October 30, 2014
Accepted: January 15, 2015
Published: January 23, 2015

DOI: 10.1021/am507559d
ACS Appl. Mater. Interfaces 2015, 7, 2561−2568

patterns having a width of 800 nm and the width of parallelepipeds (400 nm, 800 nm, and 5 μm with the SR of 1). In addition, the adhesion effect of material properties was studied using two different materials of soft PUA (soft polyurethane acrylate, elastic modulus of 19.8 MPa) and hard PUA (hard polyurethane acrylate, elastic modulus of 320 MPa).[30] It was observed that the normal and shear adhesion forces were maximized with parallelepiped interlocking between microlines (width 5 μm, AR 2, and SR 1) made by soft PUA, which was mediated by the attractive van der Waals force. This microzip device exhibited a high repeatability (>1000 cycles) while maintaining its substantial adhesion forces in both the shear (~29.6 N cm^{-2}) and normal (~8.51 N cm^{-2}) direction, which has not been achieved by previous polymeric adhesive devices such as fabric Velcro (~9.6 N cm^{-2} in the shear direction and ~5.9 N cm^{-2} in the normal direction),[31] gecko-like polymer-based dry adhesive (~10 N cm^{-2} in the shear direction and ~5 N cm^{-2} in the normal direction),[22] and nanohairy interlocker (~40 N cm^{-2} only in the shear direction).[13,32] The theoretical analysis for van der Waals force-mediated interlocking and structural robustness against critical failures such as buckling and fracture was done and found to be in agreement with experimental data. As one practical application, a flexible electric connector was demonstrated by using our repeatable interlocking with 30 nm Pt-coated line arrays, which maintained its electrical connection and substantial adhesion force (~18 N cm^{-2}).

2. EXPERIMENTAL DETAILS

Fabrication of Line Array Patterns. The entire fabrication process of line array structures by UV-curable material is summarized in Supporting Information Figure S1. First, the silicon masters engraved with various types of line arrays were fabricated by the conventional photolithography and reactive ion etching (RIE) process. The surface of the silicon master was treated with octafluorocyclobutane (C_4F_8) gas in the inductively coupled plasma (ICP) chamber for the detachment of cured polymers. To fabricate the first replica, poly(dimethylsiloxane) (PDMS) precursor mixed with 10 wt % of curing agent (Sylgard 184, Dow Corning, U.S.A.) was poured onto the silicon mold. After the degassing process in a vacuum chamber, it was cured at 70 °C for 1 h and the PDMS replica was carefully peeled off from the silicon master mold. Here, PDMS mold was used to easily replicate PUA structure by taking advantage of its low surface energy. Then, two types of UV-curable PUA prepolymers (soft-PUA; PUA MINS 311 RM, hard-PUA; PUA MINS 301 RM, purchased from the Minuta Tech, Korea) were prepared to make line arrays for the microzip fastener. A drop of PUA was dispensed onto the PDMS mold, and a urethane-coated polyethylene terephthalate (PET) film (50 μm thickness) was slightly pressed against the liquid drop to be used as a supporting layer. The precursor was exposed to UV light (Fusion Cure System, Minuta Tech, Korea) during the curing time of about 60 s. After exposure, it was detached from the PDMS mold by peeling off the substrate.

Adhesion Test. The adhesion test was conducted by the custom-built equipment (Supporting Information Figure S2). The normal and shear adhesion forces, corresponding to the maximum force between two adhered samples at the point of detachment, were measured by using force sensors of the measurement system. The sample could be easily engaged with the alignment marks and the observation of changed optical grating (see Supporting Information Figure S3 for details) and loaded with a preload in the normal direction up to 10 N cm^{-2}. The normal and shear adhesion forces were measured at least 10 times for each case, and the averaged value was used (error bars in graph indicate standard deviation). During the measurements, the temperature of the stage was maintained at 20 °C and the relative humidity of the ambient air was about 40%. In particular, the sample was pulled at a loading rate of 0.2 mm s^{-1} in the case of the shear adhesion test in consideration of the viscoelastic property of soft-PUA (see Supporting Information Figure S4 for details).

Field-Emission Scanning Electron Microscopy (FE-SEM). SEM images were obtained by Auriga (Carl Zeiss, Germany) and S-4800 (Hitachi, Japan). To avoid charging effects, samples were coated with a Pt film about ~5 nm thick prior to measurements.

Atomic Force Microscopy (AFM). AFM images were taken by a XE-150 (Park Systems, Korea) in noncontact mode. The scan rate was 0.6 Hz, and scan resolution was 256 × 256 pixels.

Measurement of Electrical Characteristics. Real-time resistance measurement was performed using PXI-4071 digital multimeter (National Instruments, U.S.A.). I–V characteristics of the Pt-coated microzip fastener were measured by 2611A SYSTEM Source-meter (Keithley Instruments, U.S.A.). The voltage was swept from −2 to 2 V, and the resolution was 0.01 V.

3. RESULTS AND DISCUSSION

Figure 1a shows the fabrication method of a repeatable submicron- and microzipper using polymeric line arrays. It can

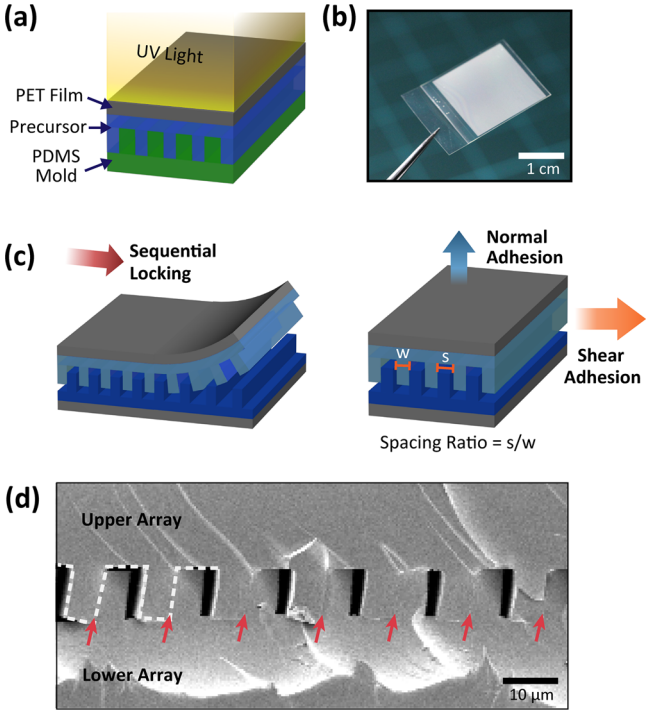

Figure 1. (a) Schematic of the fabrication process of the line arrays using UV-curable polymers. (b) An image of a microzip fastener of 5 μm in width, 10 μm in height, and spacing ratio (SR; defined as the ratio of line spacing (s) to line width (w)) of 1. (c) Illustration of the operation procedures of a microzip fastener in the normal and shear directions. (d) Cross-sectional scanning electron microscope (SEM) image of the zipperlike interlocking of polymeric rectangular parallelepiped arrays. Arrows indicate the contacts between two line structures.

be produced in a facile manner by simple replica molding with a panel of 2 × 2 cm^2 as shown in Figure 1b (see the experimental section and Supporting Information Figure S1 for details). Using the as-fabricated line array structures, the repeatable fastening procedure of submicron- and microzipper is illustrated in Figure 1c. Here, the mechanical interlocking between the identical polymeric rectangular parallelepiped arrays occurred as shown in the corresponding cross-sectional

DOI: 10.1021/am507559d
ACS Appl. Mater. Interfaces 2015, 7, 2561−2568

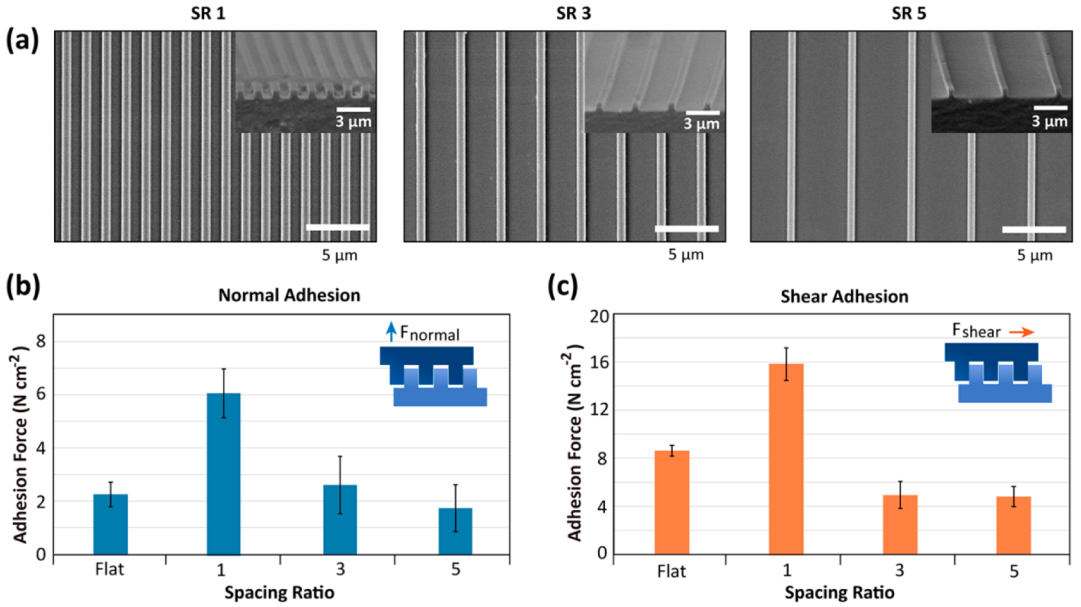

Figure 2. (a) SEM images of the 800 nm line arrays with three different spacing ratios (1, 3, and 5). The inset shows tilted view of each array. (b, c) Measured normal and shear adhesion forces between two samples. Flat-to-flat adhesion data are also plotted for comparison.

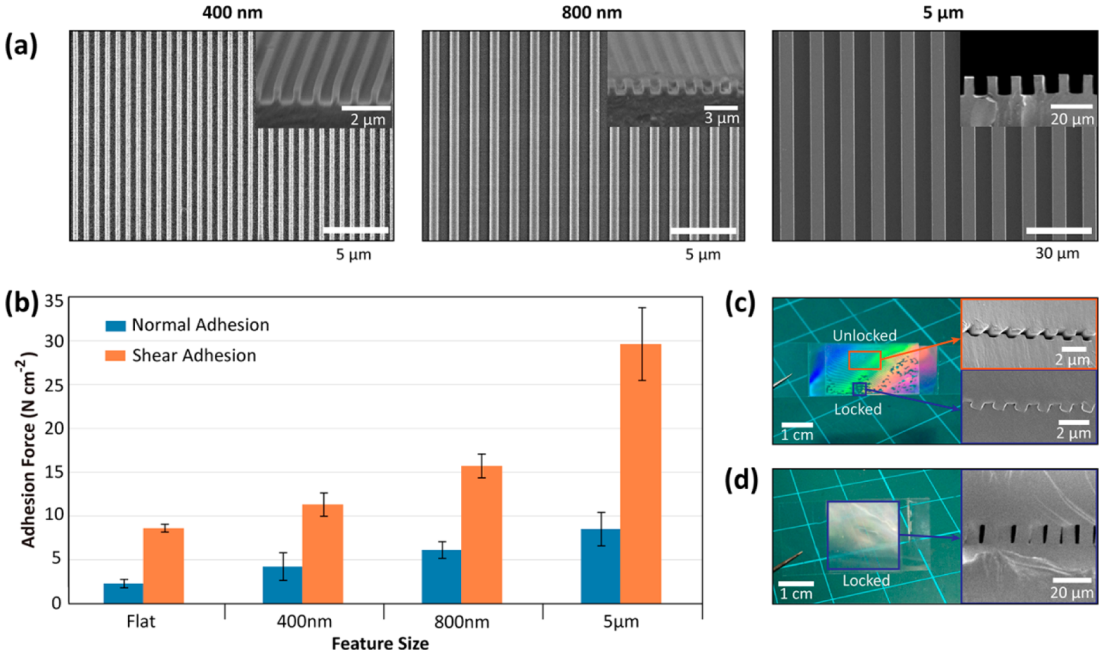

Figure 3. (a) SEM images of line array with three different width of parallelepipeds (400 nm, 800 nm, and 5 μm) with SR of 1. The inset images show tilted view of each array. (b) Normal and shear adhesion forces with submicron- and microzip fasteners (400 nm, 800 nm, and 5 μm in width). (c, d) Photographs showing (c) a misaligned zipperlike device with 800 nm lines and (d) a uniformly interlocked microzip fastener with 5 μm lines and the corresponding cross-sectional SEM images.

image of Figure 1d and Supporting Information Figure S5 (5 μm in width, 10 μm in height, and SR of 1).

To find out the apt geometry of the zipperlike connection, we measured the normal and shear adhesion forces of various line arrays with different gaps between the structures (SR: 1, 3, and 5). The width of the line structures was fixed as 800 nm (Figure 2a). After the line arrays brought into contact by the external preload (~10 N cm^{-2}), the shear and normal adhesion forces were measured with a custom-built measurement system (Supporting Information Figure S2). Interestingly, in the case of submicron-zipper with SR 1, the normal and shear adhesions were significantly enhanced (~6.1 N cm^{-2} in the normal direction and ~15.7 N cm^{-2} in the shear direction) whereas the normal and shear adhesion forces with a longer spacing (SR of 3 and 5) are even less than the flat-to-flat adhesion force (~2.3 N cm^{-2} in the normal direction and ~8.6 N cm^{-2} in the shear direction) as shown in Figure 2b and c. These results indicate that the line arrays with small spacing (SR 1) exhibited high adhesions, since the small spacing is equivalent to higher density and more line-to-line interlocking contacts per unit area. However, a line array with extremely high density (SR <1)

DOI: 10.1021/am507559d
ACS Appl. Mater. Interfaces 2015, 7, 2561−2568

is not suitable for the occurrence of interlocking within the submicron- and microzipper due to geometrical incompatibility.

Next, we investigated adhesion properties of the repeatable submicron- and microzippers with different width of parallelepipeds structures. The adhesion forces were measured with three different widths (400 nm, 800 nm, and 5 μm with SR of 1) as shown in Figure 3a. In particular, the maximum normal and shear locking forces (~8.5 and ~29.6 N cm^{-2}, respectively) were obtained using the microzip fastener with the line width of 5 μm (Figure 3b). Based on the experiments, we found that the uniform alignment of two layers is critical for high adhesion forces. Unlike the microzipper using 5-μm-width lines, dislocations of the two layers are inevitable in the submicron zip fasteners (400 and 800 nm samples), hindering the generation of nanoscale contacts mediated by van der Waals force (Figure 3c, d and Supporting Information Figure S3). It should be noted that full engagement of submicron line patterns (400 and 800 nm in width) is beyond the level of manual manipulation. On the other hand, uniform interlocking (over 70−80% of areal fraction, which is defined as the area of interlocked region over the area of the sample) can be achieved in the microzipper using 5-μm-width lines for the patterned region, resulting in high normal and shear adhesion forces (see Supporting Information Figures S3 and S6 for details). To prevent misalignment, we employed the alignment marks (+ and −), which are simply fabricated with a photomask during the UV-curing process as shown in Supporting Information Figure S3.

In addition, the rigidity of the line patterns was demonstrated as one of the major parameters for the high adhesion and robustness of the fabricated microzip fasteners. Here, the microzip fasteners are fabricated by using two different polyurethane (PU)-based materials to analyze the effects of materials: soft PUA (polyurethane acrylate, E = 19.8 MPa) and hard PUA (E = 320 MPa). It is noted that the elastic modulus (denoted as E) of PU-based materials can be tuned by changing the component and ratio of modulator as described in earlier reports.[30,33] Here, the dimension of the samples was fixed to have the width of 5 μm and the SR of 1, which showed the highest adhesion force both in the normal and shear direction. In Figure 4a, the experimental results show that the soft PUA-based microzipper has higher adhesion force (8.51 N cm^{-2} in the normal direction and 29.7 N cm^{-2} in the shear direction) than the hard PUA-based device (1.16 N cm^{-2} in the normal direction and 8.86 N cm^{-2} in the shear direction). To explain the different adhesion forces between the microstructures with soft and hard materials, we calculated the percentage of area in contact of soft and hard PUA, demonstrating that it depends on their surface roughness of microstructures as shown in Figure 4b. Namely, it is pointed out that the nanoscale roughness on the contact surface could significantly affect the percentage of area in contact,[34−36] which can provide a criterion to judge whether interlocking would take place or not with different rigidity of polymeric rectangular parallelepiped arrays. The percentage of area in nanoscale contact was critical for the high adhesion force in the overlapped region, since the van der Waals force-mediated contacts could induce mechanical interlocking on the two sidewalls of the microzip fastener (SEM images of Figure 1c). Here, the roughness of the different surfaces can be modeled using the Gaussian distribution of asperity heights as a simplified estimation.[37−39] By employing this assumption, the percentage of area in contact

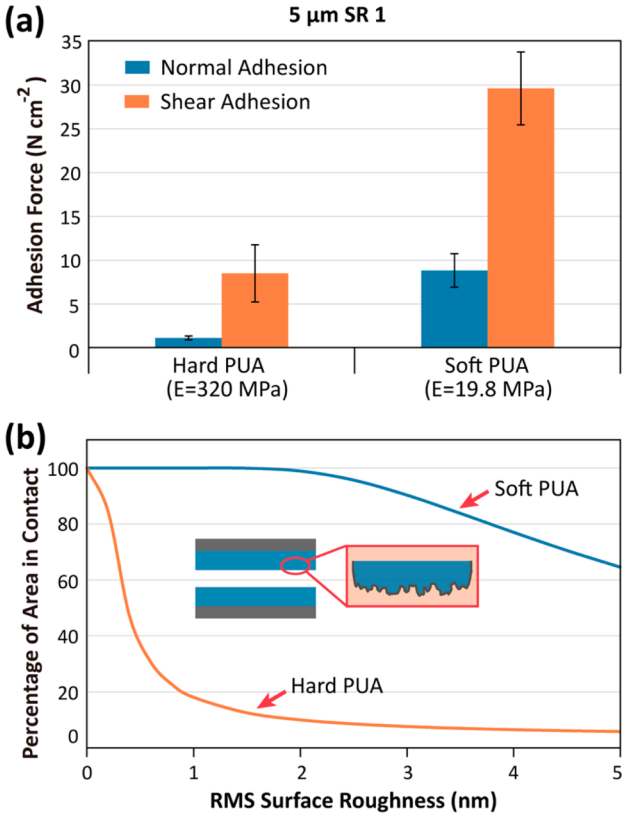

Figure 4. (a) Plots showing difference in the normal and shear adhesion forces with hard and soft PUA using line pattern with 5 μm width and SR of 1. (b) Theoretical model of the percentage of area in contact with soft and hard material depending on their roughness calculated from eqs 1 and 2.

between the two identical surfaces (C) can be derived using the error function as

$$C = \frac{1}{2}\left[\mathrm{erf}\left(\frac{\delta_1 + \delta_2 - h_{\mathrm{peak}}}{2\sigma}\right) + 1\right] \quad (1)$$

$$\delta_i = k_i\left(\frac{\sigma^{1/2}\gamma}{E^*}\right)^{2/3} \quad (2)$$

where δ_1 and δ_2 are the minimum and maximum amounts of deformation predicted by Johnson−Kendall−Roberts (JKR) contact model, h_{peak} is the maximum height of peak for the surface (~2.7 σ), σ is the root-mean-square (RMS) roughness of surface, γ is the surface energy, and E^* is the composite modulus ($E^* = E/2(1 - \nu^2)$, ν is the Poisson's ratio) of the material, respectively.[39] Since both materials have similar surface energies (19.3 mJ m^{-2} for soft PUA and 18.0 mJ m^{-2} for hard PUA, see Supporting Information for details) and RMS surface roughness (~1.96 nm, Supporting Information Figure S7), the elastic modulus would dominantly affect the probability of generating the area in contact. In our measurement, the fraction of the area in contact for the microzipper with soft PUA was estimated to ~96%, which signifies firm interconnections of the macrostructures. On the other hand, the value of C for hard PUA dramatically fell down to 7.8%.

With the interlocking generated with soft materials, the shear adhesion force of the interlocked system can be estimated by

DOI: 10.1021/am507559d
ACS Appl. Mater. Interfaces 2015, 7, 2561−2568

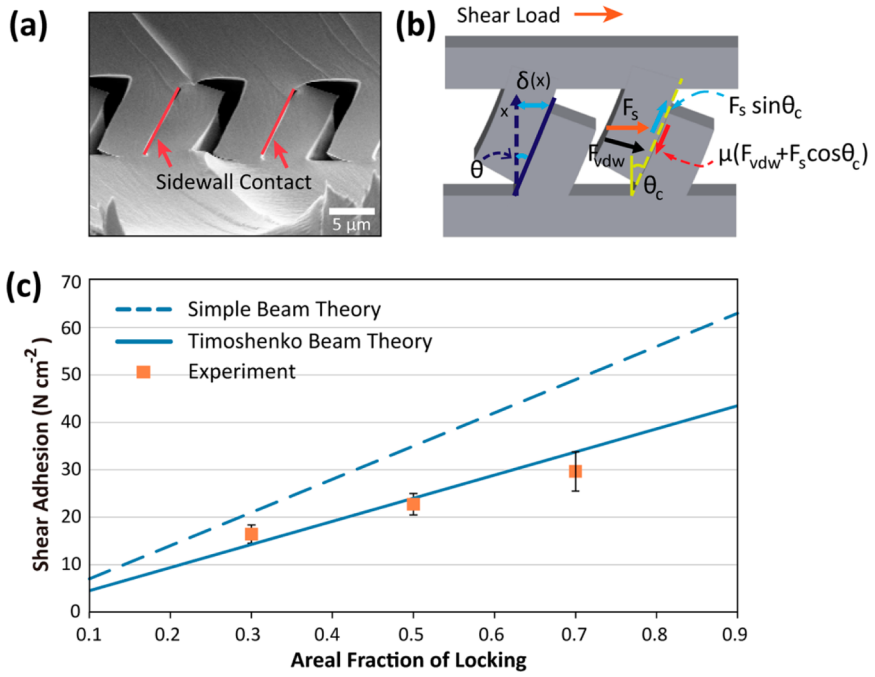

Figure 5. (a) Cross-sectional SEM image of deflected, zipped line arrays by external shear load. (b) Schematic illustration of force balance of the deflection and van der Waals force in a microzip fastener. (c) Plots of theoretical shear adhesion force predicted by the simple beam theory and the Timoshenko beam bending theory. Measured adhesion force well agreed with the Timoshenko beam bending theory.

considering the force balance of the microline arrays. Figures 5a and 5b show the underlying mechanisms of the interlocked rectangular parallelepiped arrays. As shown, the contact surface between paired structures becomes slanted as external shear load is applied. Here, the shear adhesion force of the interlocked line arrays can be determined by the competition between the frictional force at the contact surface and the disjoining force from the external load. By employing the law of friction ($F = \mu N$, μ is the frictional coefficient), a force equilibrium at single paired interlocked line structures can be established. The interlocked line structure remains merged until

$$F_s \sin\theta < \mu(CF_{vdw} + F_s \cos\theta) \tag{3}$$

where F_s is the external shear force applied to the single paired structures and F_{vdw} is the van der Waals force between two surfaces. Here, the van der Waals force can be written as $F_{vdw} = A_H/6\pi D_0^3$ per unit area,[40] where A_H denotes the Hamaker constant (2.09×10^{-20} J for soft PUA),[13] and D_0 is the cutoff distance which is assumed to be 0.4 nm.[34,40] The paired structures would begin to be separated when the inclined angle reaches a critical value (θ_c) that satisfies the criteria below.

$$F_s \sin\theta_c = \mu(CF_{vdw} + F_s \cos\theta_c) \tag{4}$$

Here, the critical angle θ_c can be approximated on the basis of the geometric relation between the line height (L) and maximum deflection (δ_{max}) of the structure ($\theta_c \approx \delta_{max}/L$). In eq 4, the deflection angle of merged line structures is a critical parameter for the prediction of the shear adhesion force. The simple beam theory (or the Euler–Bernoulli beam theory), which is frequently used to estimate the deflection of beam structures, is not appropriate in low AR arrays because it underestimates the deflection of the structure by neglecting the transverse shear effect. Therefore, we adopted the Timoshenko beam bending theory which takes into account the transverse shear force to properly calculate the deflection and bending angle (θ_c) of our low AR line structures (see Supporting Information for detailed explanation). In detail, the deflection predicted by the Timoshenko beam theory (δ^T) can be expressed with the amount of beam deflection derived by the simple beam theory (δ^T) and the additional term as below.

$$\delta^T = \delta^E + \frac{(M^E - M_0^E)}{GA\kappa_s} \tag{5}$$

where M is the bending moment, M_0 is the bending moment at the base, G is the shear modulus ($G = E/2(1 + \nu)$, ν is the Poisson's ratio), A is the cross-sectional area, κ_s is the shear correction coefficient ($\kappa_s = ((5 + 5\nu)/(6 + 5\nu))$ for rectangular cross-section[41]), and superscripts T and E indicate that the corresponding term is based on the Timoshenko beam theory and the Euler–Bernoulli beam theory.[42]

By assuming uniform distribution of external load across the contact area, the maximum deflection at the tip derived by the Timoshenko beam theory can be expressed as

$$\delta_{max} = 2F_sL\left(\frac{L^2}{48EI}\frac{(3 - (1 - \alpha)^3(3 + \alpha))}{\alpha} + \frac{2 - \alpha}{GA\kappa_s}\right) \tag{6}$$

where I is the second moment of inertia and α is the overlap ratio (α = overlapped length/line height) (see Supporting Information and Supporting Information Figure S8 for details). From our observation of the interlocked arrays, the average value of α was estimated as 0.8 (Supporting Information Figure S5). By substituting θ_c to eq 4, the shear adhesion force of single microstructure (F_s) was calculated as 60.5 μN when adopting the Timoshenko beam theory. On the other hand, F_s was estimated to be higher (87.5 μN) when adopting the simple beam theory without the transverse shear effect. As plotted in Figure 5c, experimental results of the adhesion force with changing the area fraction of locking correspond well with

DOI: 10.1021/am507559d
ACS Appl. Mater. Interfaces 2015, 7, 2561−2568

the Timoshenko beam bending theory (solid line) rather than the simple beam bending theory (dotted line).

To understand the structural features for high durability of the microzip fastener, the theoretical criteria of structural failures are characterized with applied external loads in the vertical and shear directions. Failures in line structures can occur in the form of two cases depending on the direction of external load depicted in the inset of Figure 6: (i) the buckling of structures originating from normal preload before adhesion measurements and (ii) the fracture at the bottom induced by tensile bending stress. The critical buckling and shear load that a microline structure can withstand were calculated and illustrated in Figure 6, which were produced by considering the relationship between geometrical and material properties. Limitation of applied external load can be presented through this estimation. At first, the buckling threshold shows critical preloads with varying AR of microstructures in the case of a line width of 5 μm and AR of 2 (Figure 6). In order to analyze the buckling criterion of the microzip fastener, we employed a clamped end at the bottom and a free end at the top side, which is the most conservative condition of buckling.[43] The critical buckling load of a single line structure per unit length, $F_{b,c}$, can be expressed as[43]

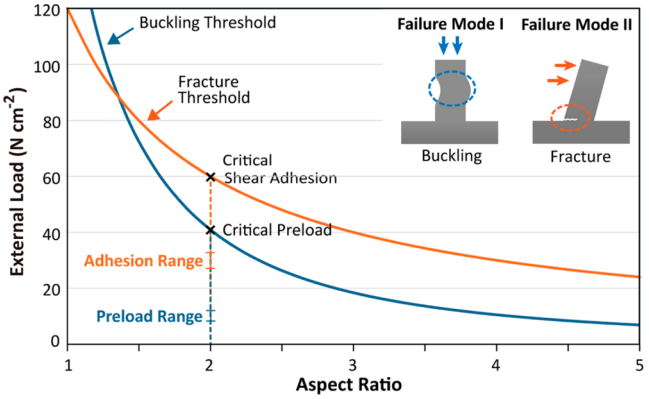

Figure 6. Mechanical analysis of buckling and fracture generation in 5-μm-width line arrays with soft-PUA (AR of 2) by different external force of preload and shear strength calculated from eqs 7 and 9. Inset images show two types of failures: buckling of microstructures by preload and fracture of lines by tensile strength.

$$F_{b,c} = \frac{\pi^2 EI}{4L^2} = \frac{\pi^2 Ebw}{48}\frac{1}{(AR)^2} \quad (7)$$

where w is the width of line structure. From eq 7, one can calculate the critical preload for the buckling failure from external load. In the case of the microzip device of 5 μm in width and the AR of 2, the critical buckling pressure was calculated as ~40.7 N cm^{-2}. It indicates that line structures of the microzip are more stable even in the condition of high load, compared with the case of micropillar fasteners (Supporting Information Figure S9). In addition, the tensile threshold is another factor that should be considered for stability assess-

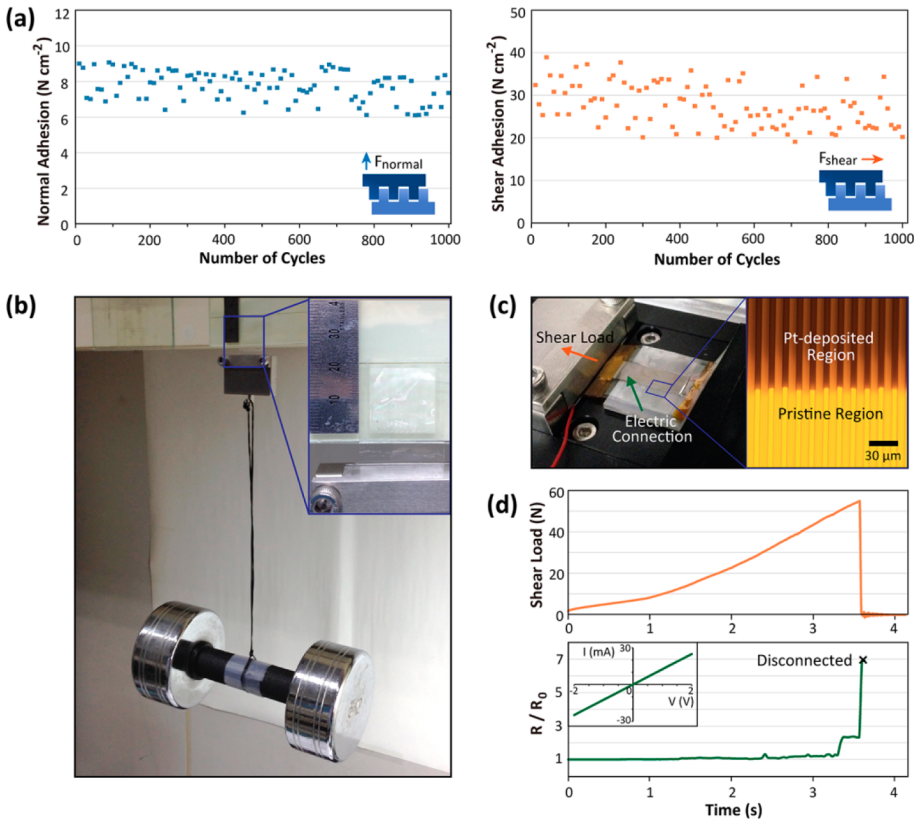

Figure 7. (a) Durability of a microzip fastener with multiple cycles of repeatable attachment and detachment up to 1000 cycles. (b) Photograph showing a 5 kg dumbbell suspended by a microzip fastener. (c, d) Practical application of a microzip fastening device as an electric connector with a thin coating of Pt (30 nm). (c) Photograph of the experimental setup and microscope image of partially coated electrical microzipper. (d) Recorded shear adhesion force and normalized resistance, showing robust electric connection. Inset is measured I–V characteristics of electrical microzipper before applying external load.

DOI: 10.1021/am507559d
ACS Appl. Mater. Interfaces 2015, 7, 2561−2568

ment. The tensile stress (σ_b) caused by the external shear force can be expressed as[43]

$$\sigma_b = \frac{M_b y}{I} \quad (8)$$

where M_b is the bending moment at the section and y is the distance from the neutral axis. By assuming the distributed load condition, the critical external shear load ($F_{t,c}$) of the line structure with unit length is obtained as

$$F_{t,c} = \frac{w\sigma_u}{3}\frac{1}{(AR)} \quad (9)$$

where σ_u is the ultimate tensile stress of the soft PUA (~9 MPa).[33] $F_{t,c}$ was calculated as about 60 N cm^{-2}, which is about two times higher than the measured shear adhesion range of 29.6 ± 4.15 N cm^{-2} (see Figure 3b). Consequently, failures in the whole structure are hardly expected during multiple cycles of the attachment and detachment process. In accordance with the theoretical analysis, the simple microzip fastener shows high durability and stability during the experimental cycle tests (>1000) of the normal and shear adhesion (Figure 7a). The degradation in the normal and shear adhesion force was not observed throughout the experiment, and the structural solidity was verified by the SEM image after the repeatability test (Supporting Information Figure S10). Our result also implies that a proper selection of the material and design of structures can lead to more optimized adhesion system.

Finally, we demonstrated the potential applications of the simple microzip fastener. First, a 5 kg dumbbell was stably suspended using the microzip device (2 cm × 2 cm, Figure 7b), indicating that the line interlocker has sufficient adhesion capability as a practical system. Moreover, a microzip fastener can also be used as a repeatable electric connector with the partial deposition of platinum (Pt, ~30 nm thickness) (Figures 7c and 7d). As shown in Figure 7d, the interlocked system maintained its substantial adhesion force (~18 N cm^{-2}) and stable electric connection (~80 Ω for 15 mm × 7 mm contact area) until failure. While the performance is similar to that of the recently introduced electric connector based on a Ge-based nanowire forest,[44] the cost-effective large-area microzip fastener securing such characteristics could play a prominent role in the field of microelectronics and flexible electronics in terms of providing both mechanical and electric connection on the flexible film-type substrate.

4. CONCLUSION

In this paper, we presented a highly robust and repeatable microzip fastening system using regularly arrayed line array structures. The rectangular parallelepiped array was fabricated with a simple UV-assisted molding technique, which does not involve any complicated physical structures or chemicals such as hierarchical assemblies or additional surface treatments. The experimental and theoretical studies demonstrated that the ziplike, van der Waals force assisted interlocking resulted in high adhesion forces both in the normal (~8.51 N cm^{-2}) and shear (~29.6 N cm^{-2}) direction. In addition, highly repeatable adhesion (>1000 cycles) was achieved without any notable degradation of line microstructures. The simple model for the stability of the microzip fastener was developed in two different modes with respect to buckling and tensile strength. In accordance with the development of various bioinspired dry adhesives, this study on the robust microzip fastening device can pave the way for the realization of robust and smart fastening systems for various potential applications such as stable, flexible fasteners or electric connecters.

■ ASSOCIATED CONTENT

Supporting Information

Fabrication process, adhesion testing machine, alignment process, loading rate effect, large-area SEM image, additional images, surface energy calculation, AFM roughness data, theoretical explanation of beam theory, failure estimation graph, and repeatability test. This material is available free of charge via the Internet at http://pubs.acs.org/.

■ AUTHOR INFORMATION

Corresponding Authors

*E-mail: mchoi@snu.ac.kr.
*E-mail: chpang@skku.edu.

Author Contributions

[⊥]C. Lee and S. M. Kim contributed equally to this work.

Notes

The authors declare no competing financial interest.
[‖]Deceased 29 June 2013.

■ ACKNOWLEDGMENTS

All authors deeply appreciate the late Professor Kahp-Yang Suh for his valuable contribution on this study. We thank S. M. Kang and S. Jang for useful comments. This work was supported by the Global Frontier R&D Program on Center for Multiscale Energy System funded by the National Research Foundation under the Ministry of Science, ICT & Future, Korea (2011-0031561), Samcro Hyosung Adilestari, Indonesia (2012-0420-20120053), and partially granted by the National Research Foundation (NRF-2014R1A1A1007162).

■ REFERENCES

(1) Gorb, S. N. Biological Attachment Devices: Exploring Nature's Diversity for Biomimetics. *Philos. Trans. R. Soc., A* **2008**, *366*, 1557−1574.
(2) Bhushan, B. Biomimetics: Lessons from Nature−An Overview. *Philos. Trans. R. Soc., A* **2009**, *367*, 1445−1486.
(3) Koch, K.; Bhushan, B.; Barthlott, W. Multifunctional Surface Structures of Plants: An Inspiration for Biomimetics. *Prog. Mater. Sci.* **2009**, *54*, 137−178.
(4) Szyndler, M. W.; Haynes, K. F.; Potter, M. F.; Corn, R. M.; Loudon, C. Entrapment of Bed Bugs by Leaf Trichomes Inspires Microfabrication of Biomimetic Surfaces. *J. R. Soc., Interface* **2013**, *10*, 20130174.
(5) Gorb, S. N. Frictional Surfaces of the Elytra-to-Body Arresting Mechanism in Tenebrionid Beetles (Coleoptera: Tenebrionidae): Design of Co-Opted Fields of Microtrichia and Cuticle Ultrastructure. *Int. J. Insect Morphol. Embryol.* **1998**, *27*, 205−225.
(6) Pang, C.; Kwak, M. K.; Lee, C.; Jeong, H. E.; Bae, W.-G.; Suh, K. Y. Nano Meets Beetles from Wing to Tiptoe: Versatile Tools for Smart and Reversible Adhesions. *Nano Today* **2012**, *7*, 496−513.
(7) Burrows, M.; Sutton, G. Interacting Gears Synchronize Propulsive Leg Movements in a Jumping Insect. *Science* **2013**, *341*, 1254−1256.
(8) Ko, H.; Zhang, Z.; Ho, J. C.; Takei, K.; Kapadia, R.; Chueh, Y.-L.; Cao, W.; Cruden, B. A.; Javey, A. Flexible Carbon−Nanofiber Connectors with Anisotropic Adhesion Properties. *Small* **2010**, *6*, 22−26.
(9) Ko, H.; Lee, J.; Schubert, B. E.; Chueh, Y. L.; Leu, P. W.; Fearing, R. S.; Javey, A. Hybrid Core−Shell Nanowire Forests as Self-Selective Chemical Connectors. *Nano Lett.* **2009**, *9*, 2054−2058.

DOI: 10.1021/am507559d
ACS Appl. Mater. Interfaces 2015, 7, 2561−2568

(10) Veedu, V. P.; Cao, A.; Li, X.; Ma, K.; Soldano, C.; Kar, S.; Ajayan, P. M.; Ghasemi-Nejhad, M. N. Multifunctional Composites Using Reinforced Laminae with Carbon−Nanotube Forests. *Nat. Mater.* **2006**, *5*, 457−462.
(11) Qu, L.; Dai, L. Gecko-Foot-Mimetic Aligned Single-Walled Carbon Nanotube Dry Adhesives with Unique Electrical and Thermal Properties. *Adv. Mater.* **2007**, *19*, 3844−3849.
(12) Rong, Z.; Zhou, Y.; Chen, B.; Robertson, J.; Federle, W.; Hofmann, S.; Steiner, U.; Goldberg-Oppenheimer, P. Bio-Inspired Hierarchical Polymer Fiber−Carbon Nanotube Adhesives. *Adv. Mater.* **2014**, *26*, 1456−1461.
(13) Pang, C.; Kim, T.-i.; Bae, W. G.; Kang, D.; Kim, S. M.; Suh, K.-Y. Bioinspired Reversible Interlocker Using Regularly Arrayed High Aspect-Ratio Polymer Fibers. *Adv. Mater.* **2012**, *24*, 475−479.
(14) Chen, C.-M.; Chiang, C.-L.; Lai, C.-L.; Xie, T.; Yang, S. Buckling-Based Strong Dry Adhesives via Interlocking. *Adv. Funct. Mater.* **2013**, *23*, 3813−3823.
(15) Shahsavan, H.; Zhao, B. Conformal Adhesion Enhancement on Biomimetic Microstructured Surfaces. *Langmuir* **2011**, *27*, 7732−7742.
(16) Kim, S.; Wu, J.; Carlson, A.; Jin, S. H.; Kovalsky, A.; Glass, P.; Liu, Z.; Ahmed, N.; Elgan, S. L.; Chen, W.; Ferreira, P. M.; Sitti, M.; Huang, Y.; Rogers, J. A. Microstructured Elastomeric Surfaces with Reversible Adhesion and Examples of Their Use in Deterministic Assembly by Transfer Printing. *Proc. Natl. Acad. Sci. U.S.A.* **2010**, *107*, 17095−17100.
(17) Kim, S.; Su, Y.; Mihi, A.; Lee, S.; Liu, Z.; Bhandakkar, T. K.; Wu, J.; Geddes, J. B.; Johnson, H. T.; Zhang, Y.; Park, J.-K.; Braun, P. V.; Huang, Y.; Rogers, J. A. Imbricate Scales as a Design Construct for Microsystem Technologies. *Small* **2012**, *8*, 901−906.
(18) Jin, X.; Strueben, J.; Heepe, L.; Kovalev, A.; Mishra, Y. K.; Adelung, R.; Gorb, S. N.; Staubitz, A. Joining the Un-Joinable: Adhesion between Low Surface Energy Polymers Using Tetrapodal ZnO Linkers. *Adv. Mater.* **2012**, *24*, 5676−5680.
(19) Vajpayee, S.; Khare, K.; Yang, S.; Hui, C.-Y.; Jagota, A. Adhesion Selectivity Using Rippled Surfaces. *Adv. Funct. Mater.* **2011**, *21*, 547−555.
(20) Chan, E. P.; Smith, E. J.; Hayward, R. C.; Crosby, A. J. Surface Wrinkles for Smart Adhesion. *Adv. Mater.* **2008**, *20*, 711−716.
(21) Lin, P.-C.; Vajpayee, S.; Jagota, A.; Hui, C.-Y.; Yang, S. Mechanically Tunable Dry Adhesive from Wrinkled Elastomers. *Soft Matter* **2008**, *4*, 1830−1835.
(22) Jeong, H. E.; Suh, K. Y. Nanohairs and Nanotubes: Efficient Structural Elements for Gecko-Inspired Artificial Dry Adhesives. *Nano Today* **2009**, *4*, 335−346.
(23) McMeeking, R. M.; Ma, L.; Arzt, E. Mechanism Maps for Frictional Attachment between Fibrillar Surfaces. *J. Appl. Mech.* **2009**, *76*, 031007−031007.
(24) Glassmaker, N. J.; Jagota, A.; Hui, C.-Y.; Kim, J. Design of Biomimetic Fibrillar Interfaces: 1. Making Contact. *J. R. Soc. Interface* **2004**, *1*, 23−33.
(25) Greiner, C.; del Campo, A.; Arzt, E. Adhesion of Bioinspired Micropatterned Surfaces: Effects of Pillar Radius, Aspect Ratio, and Preload. *Langmuir* **2007**, *23*, 3495−3502.
(26) Spolenak, R.; Gorb, S.; Arzt, E. Adhesion Design Maps for Bio-Inspired Attachment Systems. *Acta Biomater.* **2005**, *1*, 5−13.
(27) Jeong, H. E.; Lee, J.-K.; Kim, H. N.; Moon, S. H.; Suh, K. Y. A Nontransferring Dry Adhesive with Hierarchical Polymer Nanohairs. *Proc. Natl. Acad. Sci. U.S.A.* **2009**, *106*, 5639−5644.
(28) Kim, T.-i.; Jeong, H. E.; Suh, K. Y.; Lee, H. H. Stooped Nanohairs: Geometry-Controllable, Unidirectional, Reversible, and Robust Gecko-Like Dry Adhesive. *Adv. Mater.* **2009**, *21*, 2276−2281.
(29) Yoon, H.; Kwak, M. K.; Kim, S. M.; Sung, S. H.; Lim, J.; Suh, H. S.; Suh, K. Y.; Char, K. Polymeric Nanopillars Reinforced with Metallic Shells in the Lower Stem Region. *Small* **2011**, *7*, 3005−3010.
(30) Choi, S.-J.; Kim, H. N.; Bae, W. G.; Suh, K.-Y. Modulus- and Surface Energy-Tunable Ultraviolet-Curable Polyurethane Acrylate: Properties and Applications. *J. Mater. Chem.* **2011**, *21*, 14325−14335.
(31) Velcro www.torstamp.com/Brochures/BR-122.pdf (accessed May 2014).
(32) Pang, C.; Kang, D.; Kim, T.-i.; Suh, K.-Y. Analysis of Preload-Dependent Reversible Mechanical Interlocking Using Beetle-Inspired Wing Locking Device. *Langmuir* **2011**, *28*, 2181−2186.
(33) Yoo, P. J.; Choi, S.-J.; Kim, J. H.; Suh, D.; Baek, S. J.; Kim, T. W.; Lee, H. H. Unconventional Patterning with a Modulus-Tunable Mold: From Imprinting to Microcontact Printing. *Chem. Mater.* **2004**, *16*, 5000−5005.
(34) Rabinovich, Y. I.; Adler, J. J.; Esayanur, M. S.; Ata, A.; Singh, R. K.; Moudgil, B. M. Capillary Forces between Surfaces with Nanoscale Roughness. *Adv. Colloid Interface Sci.* **2002**, *96*, 213−230.
(35) Fuller, K. N. G.; Tabor, D. The Effect of Surface Roughness on the Adhesion of Elastic Solids. *Proc. R. Soc. London, Ser. A* **1975**, *345*, 327−342.
(36) Jaiswal, R. P.; Kumar, G.; Kilroy, C. M.; Beaudoin, S. P. Modeling and Validation of the Van Der Waals Force During the Adhesion of Nanoscale Objects to Rough Surfaces: A Detailed Description. *Langmuir* **2009**, *25*, 10612−10623.
(37) Nosonovsky, M.; Bhushan, B. Biologically Inspired Surfaces: Broadening the Scope of Roughness**. *Adv. Funct. Mater.* **2008**, *18*, 843−855.
(38) Greenwood, J. A.; Williamson, J. B. P. Contact of Nominally Flat Surfaces. *Proc. R. Soc. London, Ser. A* **1966**, *295*, 300−319.
(39) You, S.; Wan, M. P. Mathematical Models for the Van Der Waals Force and Capillary Force between a Rough Particle and Surface. *Langmuir* **2013**, *29*, 9104−9117.
(40) Leckband, D.; Israelachvili, J. Intermolecular Forces in Biology. *Q. Rev. Biophys.* **2001**, *34*, 105−267.
(41) Kaneko, T. On Timoshenko's Correction for Shear in Vibrating Beams. *J. Phys. D: Appl. Phys.* **1975**, *8*, 1927.
(42) Wang, C. Timoshenko Beam-Bending Solutions in Terms of Euler−Bernoulli Solutions. *J. Eng. Mech.* **1995**, *121*, 763−765.
(43) Crandall, S. H.; Lardner, T. J.; Dahl, N. C. *An Introduction to the Mechanics of Solids*; McGraw-Hill Book Company: New York, 1999.
(44) Kapadia, R.; Ko, H.; Chueh, Y.-L.; Ho, J. C.; Takahashi, T.; Zhang, Z.; Javey, A. Hybrid Core-Multishell Nanowire Forests for Electrical Connector Applications. *Appl. Phys. Lett.* **2009**, *94*, 263110.

DOI: 10.1021/am507559d
ACS Appl. Mater. Interfaces 2015, 7, 2561−2568